PTEP

Prog. Theor. Exp. Phys. **2018**, 023B06 (18 pages)
DOI: 10.1093/ptep/pty002

A novel approach to finely tuned supersymmetric standard models: The case of the non-universal Higgs mass model

Masahiro Yamaguchi* and Wen Yin*

Department of Physics, Tohoku University, Sendai 980-8578, Japan
*E-mail: yama@tuhep.phys.tohoku.ac.jp; yinwen@tuhep.phys.tohoku.ac.jp

Received August 5, 2017; Revised December 18, 2017; Accepted January 3, 2018; Published February 24, 2018

Discarding the prejudice about fine tuning, we propose a novel and efficient approach to identify relevant regions of fundamental parameter space in supersymmetric models with some amount of fine tuning. The essential idea is the mapping of experimental constraints at a low-energy scale, rather than the parameter sets, to those of the fundamental parameter space. Applying this method to the non-universal Higgs mass model, we identify a new interesting superparticle mass pattern where some of the first two generation squarks are light whilst the stops are kept heavy as 6 TeV. Furthermore, as another application of this method, we show that the discrepancy of the muon anomalous magnetic dipole moment can be filled by a supersymmetric contribution within the 1σ level of the experimental and theoretical errors, which was overlooked by previous studies due to the extremely fine tuning required.

Subject Index B13, B32, B40, B42, B58

1. Introduction

Although the discovery of the Higgs boson in July 2012 verifies our thought that the physics up to the electroweak scale should be well described by the standard model (SM) of particle physics [1,2], the SM itself suffers from the uncomfortably large disparity between the electroweak scale and the fundamental physics scale, which is supposedly close to the Planck scale. Supersymmetry (SUSY) has been recognized as a promising candidate to solve this difficulty. The fact that superparticles have not yet been discovered, however, constrains their mass spectra, if they exist; e.g., colored superparticles should weigh at least around 1 TeV [3,4]. In the minimal supersymmetric standard model (MSSM), the measured Higgs boson mass of about 125 GeV requires large radiative corrections due to supersymmetry breaking (SUSY breaking) to raise its tree-level mass below the Z boson mass [5–7]. As the Higgs boson strongly couples to the top-stop sector, this typically requires that the stop mass has to be around 6 TeV or so, unless a SUSY-breaking trilinear coupling is parametrically large [8–12]. In this case, there will be a little hierarchy between the electroweak scale and SUSY-breaking mass parameters, and thus some amount of fine tuning among these parameters may be requisite in order that electroweak symmetry breakdown takes place at the correct energy scale.

This situation does not mean that nature rejects SUSY, but implies that we should not have a prejudice against the amount of fine tuning. Since SUSY is still a promising candidate for physics beyond the SM, we should study the supersymmetric SM with some amount of fine tuning (FT-SUSY: finely tuned supersymmetry).

To identify an experimentally viable region or an interesting region of a model, the scatter-plot method has been widely used. This method represents a relevant region by a collection of discretized

Funded by SCOAP[3]

points in the fundamental parameter space, just like pointillism. The collection of points is selected from a large number of initially chosen points in the fundamental parameter space to satisfy the experimental (and other) constraints at the experimental scale.[1] However, in an FT-SUSY the relevant region might be too tiny to be represented in a way based on pointillism.

In this paper, we propose a novel approach to an FT-SUSY regardless of the amount of fine tuning.

In Sect. 2, we propose a method to identify the relevant region of an FT-SUSY. In contrast to the ordinary top-down renormalization group (RG) picture, in which a point chosen in the fundamental parameter space at the fundamental scale flows to that at the experimental scale, we map a constraint for the parameter space at the experimental scale to that at the fundamental scale. Then, we can directly identify the restricted space by the mapped constraints as the relevant region written in the fundamental parameters. This procedure is like "coloring". This procedure allows us to identify the whole relevant region as well as its outlines in the fundamental parameter space. Furthermore, the area near an outline can be easily identified as a phenomenologically interesting region, if this outline corresponds to the boundary of a constraint given by an ongoing experiment. Since the constraints we map can also include the requirement of a characteristic property, if we choose a suitable requirement, a finely tuned region is identified.

In Sect. 3, to illustrate our idea and to show its efficiency, we apply this procedure to the non-universal Higgs mass model (NUHM) [21–23], which has MSSM particle contents with universal SUSY-breaking masses except for the Higgs masses at the GUT scale. We identify the experimentally viable region of the NUHM and argue its features. We find an interesting region with a new superparticle mass pattern, where some of the first two generation squarks are light (Sect. 3.1). This mass pattern is a consequence of the RG running where a negative Higgs mass squared dominantly raises the third-generation squark masses due to their rather large Yukawa couplings. Since this effect never happens in the constrained MSSM (CMSSM), this region should be one of the characters of the NUHM (Sect. 3.2).

In Sect. 4, using another application of our method, we find that there is an extremely finely tuned region that explains the anomaly of the muon anomalous magnetic dipole moment (muon $g-2$) [24–26] within the 1σ experimental and theoretical errors in the NUHM. Furthermore, with sufficiently large $\tan\beta$, we also show that there is a parameter region explaining the muon $g-2$ anomaly with most of the first- and second-generation sfermions being light. These regions were overlooked by previous studies using the scatter-plot method, which is not practical to find such a tiny and extremely finely tuned region. This fact shows the power of our approach to an FT-SUSY.

2. A novel approach to FT-SUSY

We propose a novel approach to tackle an FT-SUSY.[2] In this approach, we can directly identify the relevant region in the FT-SUSY without being bothered with some amount of fine tuning.

For the sake of simplicity, suppose that a fundamental supersymmetric model, such as a grand unified theory (GUT), can be described as a generic MSSM. The generic MSSM is defined as an effective theory with most general SUSY-breaking soft mass parameters of the particle contents,

[1] We note that there are also several sophisticated methods other than simple random parameter scans. For reference, after χ^2 was introduced as the measure of parameter viability in Refs. [13,14], likelihood-based approaches were made to choose the sample parameters by minimizing χ^2 [15–17], and Bayesian approaches were made by defining the metric of the parameter space [18–20].

[2] In fact, the method developed here can apply to many models even without SUSY. However, for ease of explanation, we only apply our method to an FT-SUSY in this paper.

below the fundamental scale t_f of the fundamental model. t_f could be $\log\left(\frac{10^{\mathcal{O}(10)}\,\mathrm{GeV}}{m_z}\right)$ depending on the model we consider, where m_z is the Z boson mass. In the parameter space of the generic MSSM, $\mathcal{M}_f^{\rm gen}$, a point is specified by a set of $\mathcal{O}(100)$ dimensionful parameters, g_i^f at the scale t_f, where we have assumed that $\tan\beta$ is a given constant and no parameters are dimensionless. This assumption is only for simplicity and the generalization is straightforward. In contrast, the fundamental model has a restricted parameter space, the fundamental parameter space $\mathcal{M}_f^{\rm fund}$, with coordinates of much fewer fundamental parameters G_a. Since below the scale t_f, the fundamental model is described by the generic MSSM, $\mathcal{M}_f^{\rm fund}$ is embedded into a subspace of $\mathcal{M}_f^{\rm gen}$ by a set of relations:

$$g_i^f = f_i^f(G_a). \tag{1}$$

This defines a map:

$$f^f : \mathcal{M}_f^{\rm fund} \to \mathcal{M}_f^{\rm gen}, \text{ and } f^f(\mathcal{M}_f^{\rm fund}) = \left\{ g_i^f \in \mathcal{M}_f^{\rm gen} | g_i^f = f_i^f(G_a),\ G_a \in \mathcal{M}_f^{\rm fund} \right\}. \tag{2}$$

On the other hand, the solution of the RG equation (RGE) [27–29] that gives the correspondence among the parameters of the same theory at different scales can also be considered as a map $f_{\rm RG}$.[3] Since the fundamental model can be described by the generic MSSM, we consider $f_{\rm RG}$ in the context of the generic MSSM:

$$f_{\rm RG} : \mathcal{M}_f^{\rm gen} \to \mathcal{M}_e^{\rm gen}, \text{ and } f_{\rm RG}(\mathcal{M}_f^{\rm gen}) = \left\{ g_i^e \in \mathcal{M}_e^{\rm gen} | g_i^e = g_i^{\rm sol}(t_e; t_f, g_j^f),\ g_i^f \in \mathcal{M}_f^{\rm gen} \right\}. \tag{3}$$

$\mathcal{M}_e^{\rm gen}$ is the parameter space at the experimental scale $t_e = \log\left(\frac{\mathcal{O}(100)\,\mathrm{GeV}}{m_z}\right)$, and a set of $g_i^{\rm sol}(t_e; t_f, g_j^f)$ is the solution of the RG equation [27–29] in the generic MSSM at t_e with an initial condition of a set of parameters g_j^f at t_f.

Suppose that $\tilde{\mathcal{M}}_e^{\rm gen}$ denotes the region of interest of the generic MSSM at t_e, which may be either a viable region, i.e., the part of the parameter space that survives the experimental constraints, or a phenomenologically interesting region with some characteristic properties. $\tilde{\mathcal{M}}_e^{\rm gen}$ is characterized by a set of conditions expressed as $\phi_l(g_i^e) > 0$ or $\phi_l(g_i^e) = 0$:

$$\mathcal{M}_e^{\rm gen} \supset \tilde{\mathcal{M}}_e^{\rm gen} = \left\{ g_i^e \in \mathcal{M}_e^{\rm gen} | \phi_1(g_i^e) > 0, \phi_2(g_i^e) > 0, \ldots, \phi_n(g_i^e) > 0 \right\}. \tag{4}$$

Here $\phi_l(g_i^e)$ is a condition function for the generic MSSM parameters at t_e, which could either correspond to a fitted function of an experimental constraint or a requirement to have a characteristic property. The conditions in equalities, such as the ones for correct electroweak symmetry breaking and the Higgs boson mass, reduce the dimension of $\mathcal{M}_e^{\rm gen}$. On the other hand, the conditions in inequalities, such as the mass bounds for superparticles, restrict the parameter space $\mathcal{M}_e^{\rm gen}$ and hence constitute the outlines of $\tilde{\mathcal{M}}_e^{\rm gen}$. In Eq. (4), we have written down only the conditions in inequalities for illustrative purposes.

What we would like to do is to identify the region of interest at t_f, $\tilde{\mathcal{M}}_f^{\rm fund}$, in the parameter space of the fundamental model, $\mathcal{M}_f^{\rm fund}$. A conventional definition of $\tilde{\mathcal{M}}_f^{\rm fund}$ is given as

$$\mathcal{M}_f^{\rm fund} \supset \tilde{\mathcal{M}}_f^{\rm fund} = \left\{ G_a \in \mathcal{M}_f^{\rm fund} | f_{\rm RG} \circ f^f(G_a) \in \tilde{\mathcal{M}}_e^{\rm gen} \right\}. \tag{5}$$

[3] For simplicity, we suppose that $f_{\rm RG}$ is a bijection, so that the image satisfies the equality, $\mathrm{im} f_{\rm RG} \equiv f_{\rm RG}(\mathcal{M}_f^{\rm gen}) = \mathcal{M}_e^{\rm gen}$, and the inverse map, $f_{\rm RG}^{-1}$, can be defined.

Namely, given a set of the fundamental parameters, $G_a \in \mathcal{M}_f^{\rm fund}$, we apply the RG procedure to obtain the corresponding parameters at t_e, and check whether they satisfy the conditions characterizing the region of interest of the generic MSSM $\tilde{\mathcal{M}}_e^{\rm gen}$.

The ordinary scatter-plot method follows this procedure recursively by using sample points, $S = \left\{G_a^{(1)}, G_a^{(2)}, \ldots, G_a^{(N)}\right\}$, which are chosen in some way from the fundamental parameter space [15–20]. Here N is the total number of sample points. The region of interest of the fundamental model, $\tilde{\mathcal{M}}_f^{\rm fund}$, is approximated as a collection of discretized points, like pointillism. Therefore, when applying it to an FT-SUSY, in which the region of interest is so tiny, the ordinary method requires a huge number of sample points, N, as well as luck, and hence is time-consuming in numerical computation and sometimes misleading.

We now propose a novel approach to identify the region of interest, $\tilde{\mathcal{M}}_f^{\rm fund}$, in a fundamental model regardless of the amount of fine tuning that $\tilde{\mathcal{M}}_f^{\rm fund}$ has. Our definition of $\tilde{\mathcal{M}}_f^{\rm fund}$ can be written as

$$\tilde{\mathcal{M}}_f^{\rm fund} = \left\{G_a \in \mathcal{M}_f^{\rm fund} | \psi_1(G_a) > 0, \psi_2(G_a) > 0, \ldots, \psi_n(G_a) > 0\right\}, \tag{6}$$

where $\psi_l(G_a)$ is a condition function for the fundamental parameter space, expressed as

$$\psi_l(G_a) = \phi_l\left(g_i^{\rm sol}\left(t_e; t_f, f_j^f(G_a)\right)\right) = \phi_l \circ f_{\rm RG} \circ f^f(G_a), \tag{7}$$

and hence should be equivalent to Eq. (5). However, what we would like to obtain is not the correspondence among points in $\mathcal{M}_f^{\rm fund}$ and $\tilde{\mathcal{M}}_e^{\rm gen}$, but the correspondence between the two condition functions, $\phi_l(g_i^f)$ and $\psi_l(G_a)$. Namely, we map the given set of conditions, $\phi_l(g_i^e) > 0$, which characterizes $\tilde{\mathcal{M}}_e^{\rm gen}$, to the corresponding one, $\phi_l \circ f_{\rm RG}(g_i^f) > 0$, for the parameter space $\mathcal{M}_f^{\rm gen}$ at t_f within the generic MSSM, and transform the latter into the corresponding conditions in $\mathcal{M}_f^{\rm fund}$. Since the boundaries of these mapped conditions constitute the outlines of $\mathcal{M}_f^{\rm fund}$ and what we identify as $\tilde{\mathcal{M}}_f^{\rm fund}$ is the interior of the outlines, our procedure is like "coloring".

Since the map, f^f, is given, what we would like to know is the RG map of the condition function, $\phi_l(g_i^e)$, within the generic MSSM,

$$\phi_l \circ f_{\rm RG}(g_j^f) = \phi_l\left(g_i^{\rm sol}(t_e; t_f, g_j^f)\right), \tag{8}$$

and we will show how to derive the explicit form of this. One way is to solve the RG equation of the generic MSSM so that we can express $g_i^{\rm sol}(t_e; t_f, g_j^f)$ in terms of the set of the parameters g_j^f at t_f.

Alternatively, we can solve the differential equation that follows the RG map of the condition function, $\Phi_l(g_j, t) \equiv \phi_l\left(g_i^{\rm sol}(t_e; t, g_j)\right)$, by varying t:

$$\left(\frac{\partial}{\partial t} + \sum_i \beta_i \frac{\partial}{\partial g_i}\right)\Phi_l(g_j, t) = 0, \tag{9}$$

where β_i is the RG beta function for g_i [27–29].

If the perturbative expansion

$$\Phi_l(g_j, t) = \sum_{n=0} \frac{1}{n!}\phi_l^{i_1, i_2 \cdots i_n}(t) g_{i_1} g_{i_2} \cdots g_{i_n} \tag{10}$$

is allowed, a set of linear differential equations

$$\frac{\partial}{\partial t}\phi_l^{i_1, i_2 \cdots i_n}(t) = \sum_{m=1}^{n} \tilde{\beta}_{j_1, j_2 \cdots j_m}^{i_1, i_2 \cdots i_n} \phi_l^{j_1, j_2 \cdots j_m}(t), \tag{11}$$

for the coefficients, $\phi^{i_1,i_2\cdots i_n}(t)$, is derived by requiring the vanishing of each Taylor coefficient in Eq. (9). The upper limit of the summation in Eq. (11) comes from the fact that a perturbative RG beta function always contains parameters of total exponents $\geqslant 1$. Equation (11) is the running equation for coefficients of constraint (RECC) for $\phi_l(g_i^e)$. If all the parameters are dimensionful, as in our case, $\tilde{\beta}^{i_1,i_2\cdots i_n}_{j_1,j_2\cdots j_m}$ in Eq. (11) can be non-zero only if the dimension of g_i, $d(i)$, satisfies $\sum_l^n d(i_l) = \sum_l^m d(j_l)$. Hence the coefficients can be evaluated by numerically solving the derived linear differential equation.[4] We show the explicit derivation of RECC in the generic MSSM in Appendix A.

Notice that $g_i^{\rm sol}(t_e; t_f, g_i^f)$ in terms of a set of parameters, g_i^f, is obtained, once we choose a condition function $\phi_i(g_j^e) = g_i^e$. We also note that in the derivation of RECC, β_i and $\tilde{\beta}^{i_1,i_2\cdots i_n}_{j_1,j_2\cdots j_m}$ can even depend on the scale t. This is a convenient fact because we may take a shortcut to derive RECC with some parameters approximately treated as constants. Namely, if possible, we can numerically solve the RG equations for these parameters in advance, and substitute the numerical solutions as constants in the remaining RG equations. Then we can derive RECC from these remaining RG equations that explicitly depend on t. This is what we do in Appendix A.

Solving the corresponding RECCs, we can obtain the set of conditions in terms of g_i^f, $\phi_l \circ f_{\rm RG}(g_i^f) > 0$, and applying the given map, f^f, a set of $\psi_l(G_a) > 0$ is derived from Eq. (7). Therefore the whole region of interest, $\tilde{\mathcal{M}}_f^{\rm fund}$, is identified from Eq. (6).

There are two additional advantages in our approach.

Since a boundary of a constraint could correspond to an outline of $\tilde{\mathcal{M}}_f^{\rm fund}$, the viable region near such an outline may be testable if this constraint is given by an ongoing experiment. This implies that a viable region near an outline can be a phenomenologically interesting region. Therefore, checking the boundary profiles, namely, the constraints to which the boundaries correspond, we can guess some of the phenomenologically interesting regions even without any additional requirement of characteristic properties. On the other hand, the boundary profiles of a phenomenologically interesting region in turn suggest the predictions that can be accompanied by the characteristic property.[5]

The second advantage is due to the fact that in our procedure the RG map of a condition function is followed within the MSSM. In fact, we can define the region of interest of the generic MSSM at t_f:

$$\tilde{\mathcal{M}}_f^{\rm gen} = \left\{ g_i^f \in \mathcal{M}_f^{\rm gen} | \phi_1 \circ f_{\rm RG}(g_i^f) > 0, \phi_2 \circ f_{\rm RG}(g_i^f) > 0, \ldots, \phi_n \circ f_{\rm RG}(g_i^f) > 0 \right\}. \tag{12}$$

Since the viable region of the generic MSSM at t_f directly responds to the fundamental model, with stringent enough experimental constraints in the future, $\tilde{\mathcal{M}}_f^{\rm gen}$ can be a probe of the fundamental model. This approach may clarify the fundamental model directly.

3. Region of interest in the non-universal Higgs mass model

Using the method advocated in the previous section, we would like to analyze the non-universal Higgs mass model (NUHM) [21–23] as an example of a fundamental model. The NUHM is an

[4] If dimensionless parameters are included, we can also solve Eq. (11) but only perturbatively; namely, the solution can approximately represent a mapped constraint function up to a precision depending on the order of the couplings that we take into account.

[5] This may be the case with complicated constraints without approximated simplified forms, which require a lot of work to identify the relevant regions at the experimental scale. Although we can map them into those at the fundamental scale, and thus our approach is still applicable, the advantage will be quite limited.

extension of the CMSSM motivated by GUT and has universal masses for sfermions at the GUT scale $t_f \sim \log\left(\frac{2\times10^{16}\,\mathrm{GeV}}{m_z}\right)$. The only difference from the CMSSM is that in the NUHM the SUSY-breaking Higgs mass squared parameters are allowed to vary from that of sfermions at the GUT scale. This may be a natural assumption as the origin of the Higgs particles may be different from that of sfermions.

The NUHM has a fundamental parameter space, $\mathcal{M}_f^{\mathrm{fund}}$, where a point is specified by the fundamental parameters:

$$G_a = \left\{m_0^2, m_{\mathrm{Hu0}}^2, m_{\mathrm{Hd0}}^2, M_0, A_0, \mu_0, B_0\right\}. \tag{13}$$

As we have noted, $\tan\beta$, as well as the other dimensionless couplings, is taken to be a given constant that is not included in the parameter set, Eq. (13). Since the NUHM can be described by the generic MSSM below t_f, a set of fundamental parameters in $\mathcal{M}_f^{\mathrm{fund}}$ is related to the parameters in $\mathcal{M}_f^{\mathrm{gen}}$:

$$\mathbf{m}_{\tilde{\mathrm{Q}}}^2 = \mathbf{m}_{\tilde{\mathrm{u}}}^2 = \mathbf{m}_{\tilde{\mathrm{d}}}^2 = \mathbf{m}_{\tilde{\mathrm{L}}}^2 = \mathbf{m}_{\tilde{\mathrm{e}}}^2 = m_0^2\mathbf{1} \tag{14}$$

$$M_1 = M_2 = M_3 = M_0 \tag{15}$$

$$\mathbf{A}_u = \mathbf{A}_d = \mathbf{A}_e = A_0\mathbf{1} \tag{16}$$

$$m_{\mathrm{Hu}}^2 = m_{\mathrm{Hu0}}^2,\ m_{\mathrm{Hd}}^2 = m_{\mathrm{Hd0}}^2 \tag{17}$$

$$B = B_0, \mu = \mu_0. \tag{18}$$

Equations (14), (15), and (16) are the conditions of universal sfermion mass, gaugino mass, and A-term, respectively, where the bold characters are understood as three-by-three matrices of generation. Equation (17) expresses the condition of the non-universal Higgs masses at t_f, which is the only difference from the CMSSM, and also is the character of this fundamental model. The Higgs mixing parameter, μ, and the B-term are taken to be free at t_f in Eq. (18).

The experimental constraints of the generic MSSM at the experimental scale, $t_e \sim \log(\frac{100\,\mathrm{GeV}}{m_z})$, that restrict $\mathcal{M}_e^{\mathrm{gen}}$ to its viable region $\tilde{\mathcal{M}}_e^{\mathrm{gen}}$ are given:

$$2B\mu - (m_{\mathrm{Hu}}^2 + m_{\mathrm{Hd}}^2 + 2\mu^2)\sin 2\beta = 0$$

$$\mu^2 - \frac{(m_{\mathrm{Hd}}^2 - m_{\mathrm{Hu}}^2\tan^2\beta)}{\tan^2\beta - 1} - \frac{m_z^2}{2} = 0 \tag{19}$$

$$m_{\tilde{\mathrm{Q}}3}^2 \cdot m_{\tilde{\mathrm{u}}3}^2 \equiv m_{\mathrm{soft}}^4 \sim (6\,\mathrm{TeV})^4 \tag{20}$$

$$m_{\tilde{\mathrm{Q}}i,\tilde{\mathrm{u}}i,\tilde{\mathrm{d}}i}^2 > (1\,\mathrm{TeV})^2, m_{\tilde{\mathrm{L}}i,\tilde{\mathrm{e}}i}^2 > (300\,\mathrm{GeV})^2$$

$$M_3^2 > (2\,\mathrm{TeV})^2, \mu^2 > (300\,\mathrm{GeV})^2, m_{\mathrm{A}}^2 > (300\,\mathrm{GeV})^2. \tag{21}$$

Here Eqs. (19) are the constraints to obtain a correct electroweak vacuum at the tree level. Equation (20) is a rough requirement for the SM Higgs boson mass around $\sim$ 125 GeV suggested by FeynHiggs 2.11.2 [8–12]. Equations (21) are the LHC and LEP bounds of the superparticles in the MSSM [3,4]. Neglecting the first- and second-generation Yukawa couplings, the SU(2) flavor symmetry suppresses flavor violation in the sfermion sector, and we do not consider the constraints from flavor physics. Also we assume that the parameters in Eq. (13) are real and do not consider constraints of CP violation. These simplified constraints can be identified as the leading approximation of the fitting formulas or analytic formulas for the experimental constraints given in the MSSM parameter space

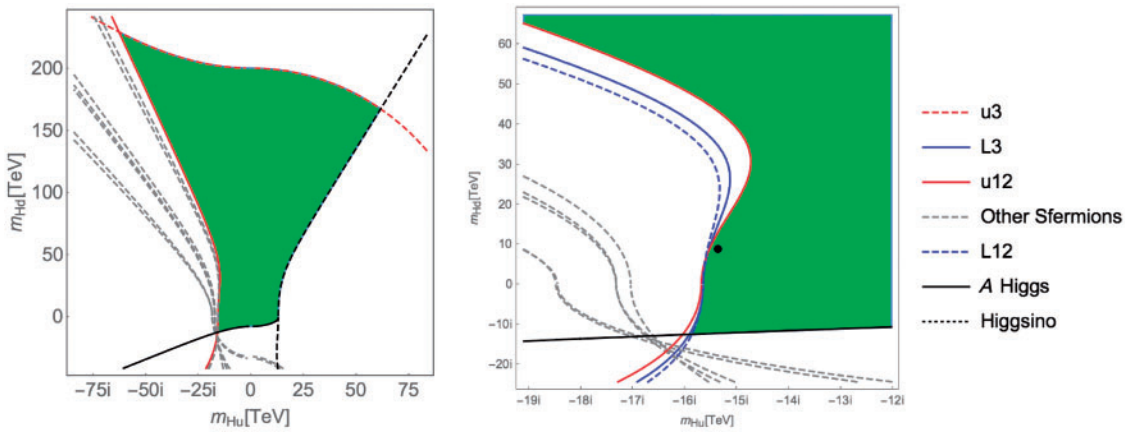

Fig. 1. The viable region and the boundaries of the experimental constraint on the slice of $M_0 = 750\,\text{GeV}$, $A_0 = 500\,\text{GeV}$ with $\tan\beta = 10$ (left). The region in green is experimentally allowed with the measured Higgs boson mass and a correct electroweak vacuum. A magnified view near an outline is presented on the right-hand side, where the boundary profiles are shown in detail. The black dot ($-15\,356i\,\text{GeV}$, 8836 GeV) represents the low-energy parameters given in Table 1.

at low energy. Since we will solve the RECCs at the one-loop level, which can be derived from the given one-loop RG equations of the MSSM as in Appendix A, we ignore the threshold corrections to the parameters. To apply a higher-loop analysis, we can include the threshold corrections in these constraints, and solve the RECCs derived from the higher-loop RG equations.[6]

3.1. Whole viable region and phenomenologically interesting regions

Solving the RECCs, which are derived from the given one-loop RG equations in Refs. [27–29] as in Appendix A, we evaluate the Taylor coefficients of the conditions, Eqs. (19), (20), and (21), in terms of the fundamental parameters, Eq. (13). Directly solving the (in)equalities for these constraints, we obtain $\tilde{\mathcal{M}}_f^{\text{fund}}$, namely, the whole viable region of the NUHM.

$\tilde{\mathcal{M}}_f^{\text{fund}}$ is characterized by four independent parameters, as the seven fundamental parameters G_a are constrained by the three equations in Eqs. (19) and (20). A 2D slice in the 4D viable region, $\mathcal{M}_f^{\text{fund}}$, is shown in Fig. 1.[7] Also shown are the mass bounds of superparticles and the pseudoscalar Higgs boson (A Higgs), where we have used the indices "12" and "3" to denote the first/second and third generations, respectively.

There is a new interesting region near the red solid line in Fig. 1, the boundary of which is given by the mass bound of the first two generation up-type squarks. We note that the stops are kept

[6] In a higher-loop analysis, the dimensionless Yukawa and gauge couplings should also be taken as fundamental parameters that depend on the spectra through matching conditions for them at the SUSY scale. Also, the constraint functions, such as the ones of the mass bounds, become more complicated in terms of the parameters in the $\overline{\text{DR}}$ scheme. In this case, our approach is applicable in analogy with the one-loop analysis, as long as we take the matching conditions of the dimensionless couplings as constraints like Eqs. (19) and (20). We can map the matching conditions as well as other complicated constraints by solving RECCs or RGEs.

[7] In fact, there are four solutions for the equations in the mapped constraints as Eqs. (19) and (20) are second order in μ_0 and m_0^2. We have chosen one of them to represent the figure, because for a given set of $\left(m_{\text{Hu0}}^2, m_{\text{Hd0}}^2, A_0, M_0\right)$, two of the solutions do not differ significantly in the one-loop analysis, and the other two have tachyonic sfermions. This fact implies an advantage of our approach, namely, the availability in the cases with multiple solutions that are difficult to identify in the ordinary top-down approach. Some of the ordinary approaches to obtain multiple solutions in simple specific models are given in Refs. [30–32].

Table 1. The low-energy parameters corresponding to the black dot ($m_{\rm Hu0}$, $m_{\rm Hd0}$, M_0, A_0) = ($-15\,400i$ GeV, 8840 GeV, 750 GeV, 500 GeV) with $\tan\beta = 10$, shown in Fig. 1. The other fundamental parameters, (m_0, μ_0, B_0) = (3200 GeV, 12 600 GeV, 1800 GeV), are evaluated from the solution of Eqs. (19) and (20). "EW" stands for electroweak.

EW scale	$m_{\rm Hu}$	$m_{\rm Hd}$	$m_{\tilde{\rm Q}3}$	$m_{\tilde{\rm u}3}$	$m_{\tilde{\rm d}3}$	$m_{\tilde{\rm L}3}$	$m_{\tilde{\rm e}3}$	$m_{\tilde{\rm Q}12}$
TeV	$-12.1i$	8.3	6.6	7.5	4.3	1.3	5.1	4.1
$m_{\tilde{\rm u}12}$	$m_{\tilde{\rm d}12}$	$m_{\tilde{\rm L}12}$	$m_{\tilde{\rm e}12}$	M_1	M_2	M_3	μ	m_A
1.6	4.4	1.4	5.2	0.31	0.62	2.2	12.2	14.9

heavy to reproduce the measured Higgs boson mass. We call this region an inverted light squark (ILSQ) region. Here "inverted" stands for the new superparticle mass pattern characterizing this region where the first two generation squarks are light, in contrast with the ordinary light stop. Table 1 illustrates the low-energy parameters corresponding to the point represented by the black dot shown in Fig. 1, where the up-type squarks in the first two generations may be within the reach of forthcoming experiments. We have confirmed that the Higgs boson mass 124(1) GeV is evaluated from FeynHiggs 2.10.2 [8–12] with the parameters in Table 1 as an input. We have also confirmed that the ILSQ region still exists including two-loop RG running by solving RECCs at the two-loop level.

Furthermore, we can observe a special point on the left-hand side of Fig. 1, where most of the contours including the gray dotted lines concentrate. Since they correspond to the mass bounds for the sfermions, the concentrating point, if near enough to the viable region, implies a surprising possibility. That is, most of the scalar masses are just above the experimental bounds in spite of the heavy stops that weigh around 6 TeV. However, as in the right-hand panel, the approximately concentrating point is too far away from the viable region, e.g., $\mathcal{O}((10\,\text{TeV})^2)$ in mass squares. In fact, the point is not excluded by the experimental mass bounds but excluded due to the unstable electroweak vacuum; namely, the A Higgs is tachyonic, $m_A^2 < 0$. We will discuss the instability in detail in Sect. 3.2, and show that it can be alleviated with large $\tan\beta$ in Sect. 4.2.

3.2. *Mechanism for the inverted light squark*

In this subsection we will explain how the characteristic mass pattern in the ILSQ region is generated in spite of the universal sfermion mass condition, Eq. (14), and the requirement of heavy stops, Eq. (20). Since these two conditions are imposed at two different scales, the RG running should be essential. The RG equation for a right-handed up-type squark mass is

$$\frac{d}{dt}m_{\tilde{\rm u}i}^2 \sim \frac{2}{16\pi^2}\left\{2y_{\rm t}^2 X_{\rm t}\delta_{i3} + Yg'^2 S - \frac{16}{3}g_3^2 M_3^2 - 4g'^2 Y^2 M_1^2\right\}, \tag{22}$$

$$S \equiv \left(m_{\rm Hu}^2 - m_{\rm Hd}^2 + {\rm Tr}[m_{\tilde{\rm Q}}^2 - m_{\tilde{\rm L}}^2 - 2m_{\tilde{\rm u}}^2 + m_{\tilde{\rm d}}^2 + m_{\tilde{\rm e}}^2]\right), \tag{23}$$

$$X_{\rm t} \equiv m_{\rm Hu}^2 + m_{\tilde{\rm Q}_3}^2 + m_{\tilde{\rm u}_3}^2 + |A_{\rm t}|^2\,, \tag{24}$$

where i represents 12 or 3, and Y is the hypercharge, $-2/3$ [27–29]. y_t is the top Yukawa coupling while g' and g_3 are gauge couplings of $\mathrm{U}(1)_{\rm Y}$ and $\mathrm{SU}(3)_{\rm c}$, respectively. The split between the third- and first-/second-generation up-type squarks should originate from the Yukawa term, the first term in Eq. (22). To raise the stop mass $m_{\tilde{u}3}$ enough for the inverted hierarchy, we need a negative and large X_t that dominates over the other terms in Eq. (22). This is realized when $m_{\rm Hu}^2$ is large and negative.

For sufficiently large $\tan\beta$, the bottom and tau Yukawa couplings can be effectively large in spite of the observed small mass ratio of bottom/tau to top. If $m_{\rm Hd}^2$ is large and negative, the same argument applies to down-type squarks and sleptons. In summary, the inverted hierarchy can be generated by the Yukawa contribution through the RG running due to a negative and large Higgs mass squared parameter.

Furthermore, we would like to explain the sfermion mass splitting within a generation. This originates in the gauge interactions, especially for $\mathrm{U}(1)_{\rm Y}$ gauge symmetry. In particular, the value of S in Eq. (23) can deviate greatly from zero in the NUHM, in contrast to the CMSSM case, where S is always zero. We find that when our mechanism of the ILSQ works, S is non-zero in order to avoid the unstable electroweak vacuum, unless $\tan\beta$ is substantially large. We show this by *reductio ad absurdum*. Suppose that $S = 0$ is satisfied with a large and negative $m_{\rm Hu0}^2$; namely, $m_{\rm Hu0}^2 = m_{\rm Hd0}^2 \ll 0$ at the GUT scale. Since X_t dominates over the other terms in Eq. (22), the RG equations of $m_{\rm Hu}^2$ and $m_{\rm Hd}^2$ are also controlled by the large and negative Higgs masses [27–29]:

$$\beta_{m_{\rm Hu}^2} \sim \frac{1}{16\pi^2} 6 y_t^2 X_t^2 \sim \frac{1}{16\pi^2} 6 y_t^2 m_{\rm Hu}^2, \tag{25}$$

$$\beta_{m_{\rm Hd}^2} \sim \frac{1}{16\pi^2} \left(6 y_b^2 m_{\rm Hd}^2 + 2 y_\tau^2 m_{\rm Hd}^2 \right). \tag{26}$$

Hence, the RG running effect decreases the absolute value of $m_{\rm Hu}^2$ at the experimental scale, while $m_{\rm Hd}^2$ does not change so much due to the smaller Yukawa couplings. This implies that at low energy

$$0 \gg m_{\rm Hu}^2 > m_{\rm Hd}^2 \tag{27}$$

is satisfied and the problem of tachyonic instability of the electroweak vacuum occurs, as $m_A^2 < 0$ by solving Eqs. (19). Therefore, we need a greater $m_{\rm Hd0}^2$ to stabilize the electroweak vacuum and hence $S < 0$. Notice that this argument depends on the sign of the Higgs mass squares and the size of $\tan\beta$. Since Eq. (25) decreases the absolute value of $m_{\rm Hu}^2$, if S is canceled by positive and large $m_{\rm Hu0}^2$ and $m_{\rm Hd0}^2$, Eq. (27) is replaced by $0 \ll m_{\rm Hu}^2 < m_{\rm Hd}^2$ and the instability problem does not occur. This is the reason why the CMSSM is allowed to have a stable electroweak vacuum. Also, if $\tan\beta$ is large enough, the RG running of $m_{\rm Hd}^2$, Eq. (26), can be effective and the vacuum instability problem should be alleviated with $S \sim 0$ in the ILSQ region.

For not so large $\tan\beta$, the property of $S < 0$ in the ILSQ region makes $\tilde{u}_{12}$ the lightest squark, as in Table 1, because it has the smallest hypercharge. The requirement of $S < 0$ is also the reason why the approximately concentrating point on the right-hand side of Fig. 1 is far away from the viable region. In fact, the approximately concentrating point lies on the line of $S = 0$ where the first two generation sfermion masses can be small without splitting. On the other hand, since $S \sim 0$ may be allowed when $\tan\beta$ is sufficiently large, in this case there is the possibility of having an ILSQ region including most of the first two sfermion masses just above the experimental bounds. This is the case in Sect. 4.2.

As we have discussed, the ILSQ region has a new superparticle mass pattern essentially related to the non-universal Higgs masses. Therefore, this mass pattern should be one of the most characteristic phenomena of the NUHM, as the CMSSM never realizes this. We note that since the stop mass in the ILSQ region is generated via the Higgs loop, there are at least three scales for the scalar mass squares: the Higgs mass scale (this can be divided into two scales corresponding to $\mathrm{H_u}$ and $\mathrm{H_d}$ with small $\tan\beta$), the stop mass scale, and the ILSQ mass scale. This hierarchy makes it difficult to identify the ILSQ region in ordinary parameter scans based on the scatter-plot method. This is because we

should set the sample points over a large parameter range to reach the large Higgs mass scale, and with high density to identify the small ILSQ scale.

4. Extremely finely tuned but important region

In Sect. 3, we have presented the whole viable region of the NUHM by solving the (in)equalities expressing the experimental constraints in terms of the fundamental parameters that can be obtained from the method advocated in Sect. 2. We have found a new phenomenologically interesting region near the boundary corresponding to a squark mass bound. However, an interesting region with a characteristic property is not necessarily around the outlines, rather inside the viable region. This is particularly the case when the characteristic property requires a fairly large amount of fine tuning among the parameters. Notice that it would be difficult for the scatter-plot method to identify such a finely tuned region.

In this section we will show how to analyze a large and complicated viable region to find out the characteristic properties localized inside it, and argue that this analysis has an advantage when applied to an FT-SUSY.

To illustrate the idea, consider here the muon anomalous magnetic dipole moment (muon $g-2$), α_μ. The muon $g-2$ anomaly is a hint of new physics, as the discrepancy between the theoretical and experimental values exceeds the 3σ level of these errors [24–26]:

$$\alpha_\mu^{\rm exp} - \alpha_\mu^{\rm SM} = (26.1 \pm 8.0) \times 10^{-10}. \tag{28}$$

In the generic MSSM at least three light superparticles, weighing around 300 GeV, are needed to generate a large enough contribution [33–35]. Therefore, the region of the generic MSSM, $\tilde{\mathcal{M}}_e^{\rm gen}$, that fills the discrepancy of the muon $g-2$, should be characterized by three parameters with very tiny values compared to the stop mass parameters around 6 TeV. Therefore, if it exists, the region of interest of the NUHM now, $\tilde{\mathcal{M}}_f^{\rm fund}$, should be finely tuned from the whole viable region in the previous section.

The particular diagram that we consider for the SUSY contribution to the muon $g-2$ is made of a loop including a bino and smuons of both chiralities [33–35]. Following Ref. [33], we obtain an approximate formula of the SUSY contribution to the muon $g-2$:

$$\begin{aligned}
\delta\alpha_\mu &\equiv \alpha_\mu^{\rm MSSM} - \alpha_\mu^{\rm SM} \\
&\sim \frac{1}{16\pi^2} \frac{g'^2 m_\mu^2 M_1 \mu \tan\beta \min\{m_{\tilde{\rm L}12}^2, m_{\tilde{\rm e}12}^2, M_1^2\}}{2 m_{\tilde{\rm L}12}^2 m_{\tilde{\rm e}12}^2 M_1^2} \\
&\sim 5 \times 10^{-10} \frac{(100\,{\rm GeV})^2 M_1 \mu \tan\beta \min\{m_{\tilde{\rm L}12}^2, m_{\tilde{\rm e}12}^2, M_1^2\}}{m_{\tilde{\rm L}12}^2 m_{\tilde{\rm e}12}^2 M_1^2}.
\end{aligned} \tag{29}$$

This rough approximation will be corrected by fitting the results evaluated in FeynHiggs 2.11.2 [8–12] by varying the overall coefficient of this function.

4.1. *How large can the muon $g-2$ be in the NUHM?*

In order to clarify whether the NUHM can explain the muon $g-2$ anomaly, an efficient way is to evaluate the maximal value of the muon $g-2$ in the NUHM. This immediately draws a conclusion of whether the muon $g-2$ anomaly can be explained. Therefore we impose a condition,

$$\text{maximize}[\delta\alpha_\mu] \text{ by varying } m_0, \tag{30}$$

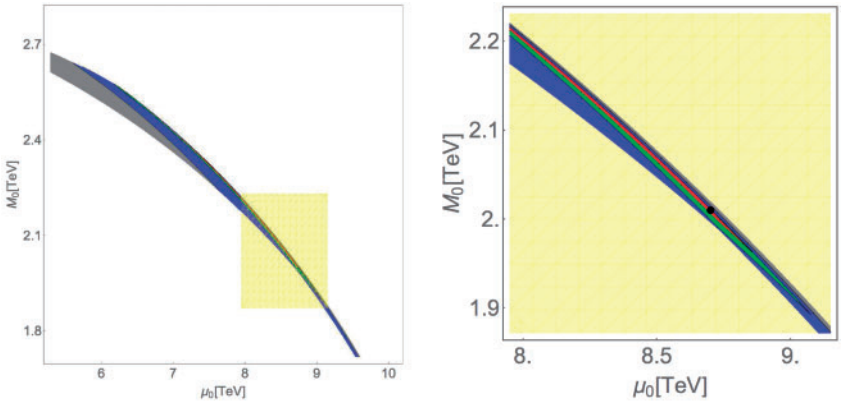

Fig. 2. A contour plot of the maximized muon $g-2$ by varying m_0 on a slice at $A_0 = 0$ with $\tan\beta = 35$ (left). A magnified view of the yellow region is presented on the right-hand side. The red (green, blue) region shows that the total muon $g-2$, including the maximal NUHM correction, is within the 1σ (2σ, 3σ) level error of the observed value. The black dot (8700 GeV, 2010 GeV) represents the low-energy parameters given in Table 2.

Table 2. The low-energy parameters corresponding to the black dot $(M_0, \mu_0, A_0) = (2010\,\text{GeV}, 8700\,\text{GeV}, 0\,\text{GeV})$ in Fig. 2 with $\tan\beta = 35$. The other fundamental parameters, $(m_0, m_{\text{Hu0}}, m_{\text{Hd0}}, B_0) = (1186i\,\text{GeV}, 9375i\,\text{GeV}, 8326i\,\text{GeV}, -768\,\text{GeV})$, are the solutions of Eqs. (19), (20), and (30). FH: FeynHiggs.

EW scale	m_{Hu}	m_{Hd}	$m_{\tilde{\text{Q}}3}$	$m_{\tilde{\text{u}}3}$	$m_{\tilde{\text{d}}3}$	$m_{\tilde{\text{L}}3}$	$m_{\tilde{\text{e}}3}$	$m_{\tilde{\text{Q}}12}$
GeV	$8044i$	$7992i$	5834	6161	5089	1637	2275	5168
$m_{\tilde{\text{u}}12}$	$m_{\tilde{\text{d}}12}$	$m_{\tilde{\text{L}}12}$	$m_{\tilde{\text{e}}12}$	M_1	M_2	M_3	$A_{\text{u}3}$	$A_{\text{d}3}$
4920	4999	429	429	839	1659	5770	−4497	−6749
$A_{\text{e}3}$	$A_{\text{u}12}$	$A_{\text{d}12}$	$A_{\text{e}12}$	μ	m_{A}	FeynHiggs	m_{h} by FH	$\delta\alpha_\mu$ by FH
−1011	−7891	−7820	−1372	8043	907	(2.11.2) [8–12]	126(1.4) GeV	2.5×10^{-9}

in addition to Eqs. (19)–(21). In fact, we can vary all the free parameters to maximize the muon $g-2$; however, for illustrative purposes we only vary one parameter. This reduces a free parameter, m_0, in $\mathcal{M}_f^{\text{fund}}$.

By solving the conditions (19)–(21) analytically, and solving the condition (30) numerically, in terms of A_0, M_0, and μ_0, we obtain a 3D region of interest, $\tilde{\mathcal{M}}_f^{\text{fund}}$. An $A_0 = 0$ slice of the solution is shown in Fig. 2 with $\tan\beta = 35$. The contours represent the maximized total muon $g-2$ by varying m_0.

We find that the maximized muon $g-2$ can exceed 18.1×10^{-10} with $\tan\beta \gtrsim 25$; namely, the NUHM is able to fill the discrepancy of the muon $g-2$ within the 1σ level error.

In fact, there are two kinds of regions, namely, type 1 and type 2 regions, depending on the lightest particle in the loop diagram corresponding to Eq. (29). The type 1 region explains the muon $g-2$ anomaly with either $\tilde{\text{e}}_{12}$ or $\tilde{\text{L}}_{12}$ as the lightest particle in this diagram, while the type 2 region has a bino as the lightest particle. Figure 2 corresponds to the former one, while the region of type 2 appears for $\tan\beta \gtrsim 55$, as we will show in Sect. 4.2.

4.2. The region explaining the muon $g-2$ anomaly and the mechanism

Since the NUHM has a region where the muon $g-2$ anomaly is explained, now we would like to explore the features of this region. Since we know that an outline may have some phenomenological

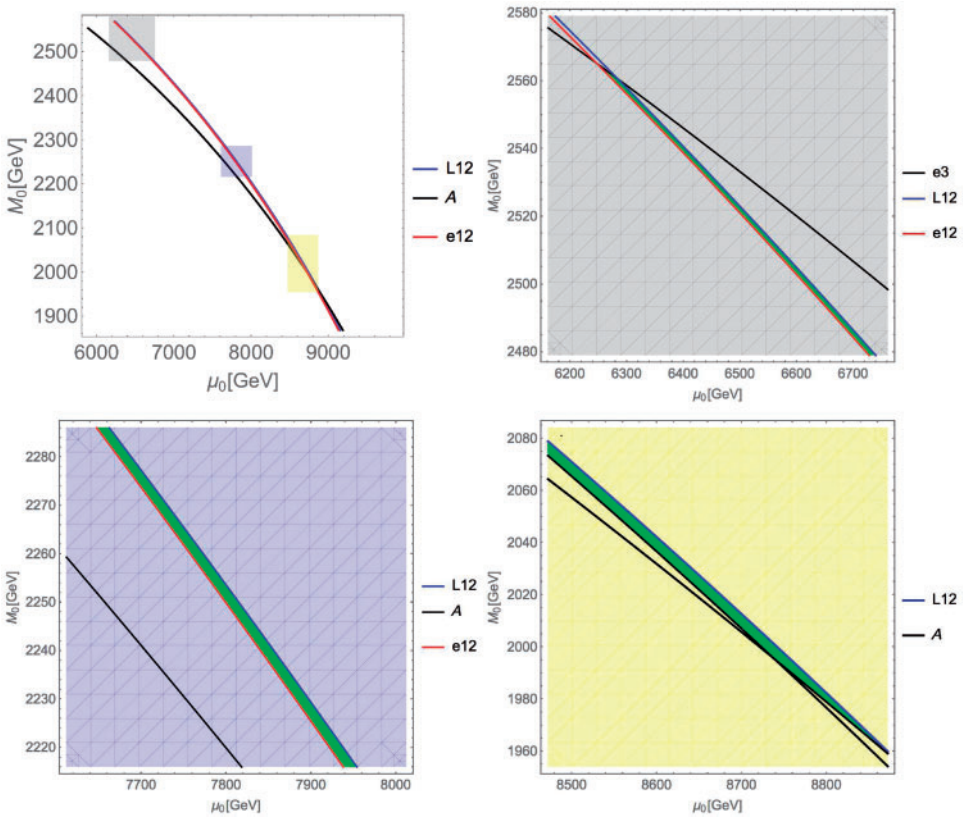

Fig. 3. $A_0 = 0$ slice of the region of type 1 with $\tan\beta = 35$. The region in green explains the muon $g-2$ anomaly within its 1σ level error where one of the smuons is lighter than the bino. A magnified view of the corresponding colored region is also shown with the boundary profiles in detail. The profiles of the boundaries that do not constitute the outlines are turned off.

information about the nearby region, it is meaningful to show the outlines of the region where the muon $g-2$ is just at the experimental central value, rather than the maximal value. We impose a condition instead of Eq. (30):

$$\frac{(100\,\mathrm{GeV})^2 M_1 \mu \tan\beta \min\{m^2_{\tilde{\mathrm{L}}12}, m^2_{\tilde{\mathrm{e}}12}, M_1^2\}}{m^2_{\tilde{\mathrm{L}}12} m^2_{\tilde{\mathrm{e}}12} M_1^2} = \begin{cases} 10\ (\tan\beta \sim 35) \\ 7.5\ (\tan\beta \sim 60). \end{cases} \tag{31}$$

The factors 10 and 7.5 on the right-hand side are fitted experimentally using FeynHiggs 2.11.2 [8–12].

The solutions by solving Eqs. (19)–(21), and (31) in terms of A_0, M_0, and μ_0, are represented in Figs. 3 and 4 corresponding to the type 1 and type 2 regions, respectively. Also shown are the boundary profiles.

If the muon $g-2$ anomaly is explained by the region in Fig. 3, from the boundary profiles we can find that some of the light smuons, selectrons, right-handed stau, and A Higgs are light. On the other hand, Fig. 4 implies that many superparticles are light, as many boundaries of the experimental constraints are within the distances of $\lesssim \mathcal{O}(\mathrm{TeV})$ from this interesting region. These regions can be tested in forthcoming experiments. A set of low-energy parameters corresponding to the type 2 region is given in Table 3. We have confirmed that the Higgs mass and the muon $g-2$ anomaly are explained using FeynHiggs 2.11.2 [8–12] with an input of these parameters. We have also confirmed that the parameter region does not vanish but shifts to a different area in the parameter space by

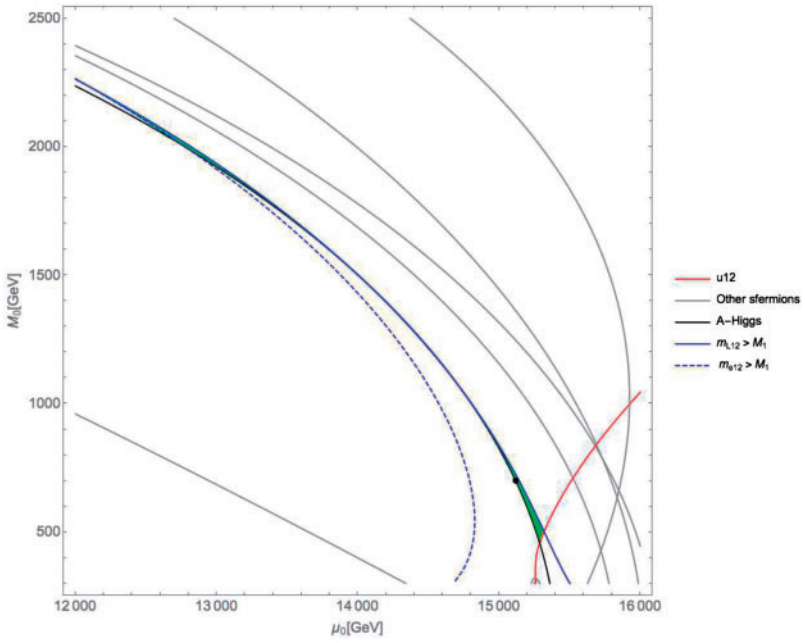

Fig. 4. $A_0 = 0$ slice of the region of type 2 with $\tan\beta = 60$. The region in green explains the muon $g-2$ anomaly within its 1σ level error where the bino is lighter than the smuons. The boundary profiles are also shown. The blue solid and dashed lines denote the boundary of the condition for having the type 2 region, which constrains the bino to be lighter than the smuons. The black dot (15120 GeV, 700 GeV) has low-energy parameters given in Table 3.

solving the RECCs at the two-loop level with some of the one-loop threshold corrections included in the conditions Eqs. (19) and (20).

Now we would like to consider how the muon $g-2$ anomaly is explained. From Eq. (31), we find that a large μ-term and a large $\tan\beta$ are favored for a large value of the muon $g-2$. This requires large and negative Higgs masses to have a correct electroweak vacuum due to Eqs. (19). Therefore the mechanism of the ILSQ in Sect. 3.2 can be applied. As noted, a negative S-term is required to stabilize the electroweak vacuum when $\tan\beta$ is not substantially large. Neglecting RG running due to gauginos, $\tilde{u}_{12}$ becomes the lightest sfermion in most of the cases as in Table 1. This excludes a smuon around 300 GeV, as it should be heavier than $\tilde{u}_{12}$, which is bounded below by 1 TeV. If we would like to decrease the smuon masses in the ILSQ region, what we should do is to increase the gluino mass. The RG effect from a heavy gluino, as the third term in Eq. (22), raises the masses of squarks universally from those of sleptons. However, the universal gaugino mass condition, Eq. (15), implies a heavy bino. Hence, the lightest particle in the loop diagram corresponding to Eq. (29) becomes a smuon, which can be seen from the boundary profiles in Fig. 3. This is the case for the type 1 region.

The type 2 region where the bino is the lightest particle in the loop diagram corresponding to Eq. (29) can be realized with sufficiently large $\tan\beta$. This is consistent with the argument noted in Sect. 3.2: $S \sim 0$ can be realized with large $\tan\beta$. In this case, we do not need a heavy gluino to raise the squark masses and the bino can be as light as the smuons. Furthermore, all the first- and second-generation sfermions will be light because small gaugino masses and S-term imply degenerate sfermions belonging to the first two generations, and the mechanism of ILSQ works for all of them. This is actually the case in Table 3.

Table 3. The low-energy parameters corresponding to the black dot $(M_0, \mu_0, A_0) = (700\,\text{GeV}, 15\,120\,\text{GeV}, 0\,\text{GeV})$ represented in Fig. 4 with $\tan\beta = 60$. The other fundamental parameters $(m_0, m_{\text{Hu0}}, m_{\text{Hd0}}, B_0) = (898\,\text{GeV}, 14\,910i\,\text{GeV}, 13\,650i\,\text{GeV}, 21\,\text{GeV})$ are obtained by solving the conditions corresponding to Eqs. (19), (20), and (31).

EW scale	m_{Hu}	m_{Hd}	$m_{\tilde{\text{Q}}3}$	$m_{\tilde{\text{u}}3}$	$m_{\tilde{\text{d}}3}$	$m_{\tilde{\text{L}}3}$	$m_{\tilde{\text{e}}3}$	$m_{\tilde{\text{Q}}12}$
GeV	$11\,820i$	$11\,780i$	6399	7553	4810	4540	6618	2125
$m_{\tilde{\text{u}}12}$	$m_{\tilde{\text{d}}12}$	$m_{\tilde{\text{L}}12}$	$m_{\tilde{\text{e}}12}$	M_1	M_2	M_3	$A_{\text{u}3}$	$A_{\text{d}3}$
1650	2146	326	1669	292	578	2010	−1511	−1998
$A_{\text{e}3}$	$A_{\text{u}12}$	$A_{\text{d}12}$	$A_{\text{e}12}$	μ	m_{A}	FeynHiggs	m_{h} by FH	$\delta\alpha_\mu$ by FH
−118	−2748	−2724	−478	11 820	946	(2.11.2) [8–12]	124.6(1.3) GeV	2.1×10^{-9}

As we can see in Figs. 2, 3, and 4, the relevant regions have small sizes due to fine tuning. In fact, fine tuning is already alleviated in these figures as we have reduced a free parameter that is finely tuned, in contrast to the stop mass scale by solving Eq. (30) or Eq. (31). On the other hand, after the discovery of the Higgs boson the muon $g-2$ correction in the NUHM has been discussed in several studies [36–39] by using the scatter-plot method utilizing several modern sampling techniques. In these studies, the tiny regions that we have identified in this paper have been overlooked, either due to the sampling range being too small or the sampling points being too sparse in the scatter-plot method (see the end of Sect. 3.2).

These finely tuned regions are easily overlooked in any analysis that has a limitation in the sampling range or the number of sampling points set by hand. We have identified them because we have focused on the physical experimental constraints without being bothered by these limitations. Therefore, we have shown that the method advocated in this paper has a strong advantage in identifying a finely tuned region and this should be an efficient approach to an FT-SUSY.

5. Conclusions

In this paper, we have proposed a novel and efficient approach to supersymmetric models with some amount of fine tuning, in which the commonly used scatter-plot approach is inefficient and sometimes even fails to find relevant regions in the parameter space of superparticle masses with the limited number of plotted points. The essential idea of our approach is to directly map the (experimental or other) constraints at low energy to those in the fundamental parameter space. We can identify the relevant region in the fundamental parameter space by filling the interior of the mapped constraints, as the boundaries of the constraints will form the outlines of the relevant region. Furthermore, the areas near the boundaries of the experimental constraints that are rather easily identified in our method could be phenomenologically interesting as they will be studied in forthcoming experiments.

We applied this method to the non-universal Higgs mass (NUHM) model. The features of the NUHM model are the same as the constrained MSSM except that the SUSY-breaking Higgs masses differ from the universal sfermion mass at the GUT scale. By using our method, we identified the phenomenologically viable regions of the parameter space and discussed some interesting features of the model. Among other things, we found, in some cases, that inverted squark masses are realized, where the renormalization group effects raise the third-generation squark masses compared to those of the first two generations. This mass pattern is a characteristic phenomenon of the NUHM model and is never realized in the constrained MSSM.

Another application of our method is to identify, within the NUHM model, the existing but tiny region in the parameter space where the SUSY contribution explains the discrepancy of the muon $g-2$ within the 1σ level of experimental and theoretical errors. The price to pay is the extremely fine tuning among the parameters, and therefore previous studies using the conventional scatter-plot method failed to find this region, drawing misleading conclusions. This example illustrates the power of our method in particular when the required fine tuning is severe. The relevance of our approach will even increase when forthcoming experiments give null results in superparticle searches and more fine tuning will be required to correctly produce the electroweak scale.

The method advocated in this paper has a variety of applications, some of which have been described in Ref. [40] and which will also be discussed elsewhere.

Acknowledgements

We would like to thank Yutaro Shoji for collaboration at an early stage of this work. This work is supported by a Grant-in-Aid for Scientific Research from the Ministry of Education, Science, Sports, and Culture (MEXT), Japan, No. 23104008.

Funding

Open Access funding: SCOAP[3].

Appendix. RECCs for the generic MSSM

We would like to show the derivation of RECCs in the generic MSSM with given dimensionless couplings at t_e. In fact, the following argument can apply to the derivation of RECCs at any loop order with a given RG equation at the same order.

The parameters g_i^f and constants of the generic MSSM are classified by their dimensions:

D = 2 Sfermion masses, Higgs masses: m_i^2
D = 1 Gaugino masses, μ- and A-terms: M_i
D = 0 Gauge couplings and Yukawa couplings: y_i

where the set of m_i^2 is understood to include the off-diagonal elements of the usual three-by-three sfermion mass matrices etc.

A perturbative RG equation for the parameters of dimension d is written in terms of the parameters with dimension $\leq d$:

$$\begin{aligned}\frac{d}{dt}m_i^2 &= a_{2,i}^k(y_j)m_k^2 + a_{1,i}^{kl}(y_j)M_kM_m,\\ \frac{d}{dt}M_i &= b_i^k(y_j)M_k,\\ \frac{d}{dt}y_i &= c_i(y_j).\end{aligned} \tag{A.1}$$

$a_{2,i}^k(y_j)$, $a_{1,i}^{kl}(y_j)$, $b_i^k(y_j)$, and $c_i(y_j)$ are given functions that can be derived from loop calculations in the generic MSSM [27–29]. The summation is understood.

Firstly, we can solve the RG equation for dimensionless constants numerically with given y_i at t_e. Substituting this numerical solution for y_i, the (effective) RG equation for dimensionful parameters

becomes

$$\frac{d}{dt}m_i^2 = a_{2,i}^k(t)m_k^2 + a_{1,i}^{kl}(t)M_kM_l$$
$$\frac{d}{dt}M_i = b_i^k(t)M_k. \tag{A.2}$$

Secondly, using Eq. (A.2), we can derive the RECCs for condition functions,

$$\phi_2(m_i^2) = m_1^2(t_e) - (10^3\ \mathrm{GeV})^2 \text{ and } \phi_1(M_i) = M_1(t_e) - (10^3\ \mathrm{GeV}), \tag{A.3}$$

corresponding to simplified experimental mass bounds of a scalar and a fermion, respectively. Dimensional analysis allows us to guess the forms of the mapped condition functions at an arbitrary scale, t, as

$$\Phi_2(t) \equiv \phi_2^i(t)m_i^2 + \phi_2^{ij}(t)M_iM_j + c_2(t) \tag{A.4}$$
$$\Phi_1(t) \equiv \phi_1^i(t)M_i + c_1(t). \tag{A.5}$$

Therefore, employing Eq. (9), the RECCs for Eqs. (A.4) and (A.5) are derived as

$$\begin{aligned}
\frac{d}{dt}\phi_2^i(t) &= -\phi_2^k(t)a_{2,k}^i(t)\\
\frac{d}{dt}\phi_2^{ij}(t) &= -\phi_2^k(t)a_{1,k}^{ij}(t) - \phi_2^{kj}(t)b_k^i(t) - \phi_2^{ik}(t)b_k^j(t)\\
\frac{d}{dt}\phi_1^i(t) &= -\phi_1^k(t)b_k^i(t)\\
\frac{d}{dt}c_1(t) &= \frac{d}{dt}c_2(t) = 0.
\end{aligned} \tag{A.6}$$

With the initial condition

$$\phi_2^i(t_e) = \delta_1^i, \phi_2^{ij}(t_e) = 0, c_2(t_e) = -(10^3\ \mathrm{GeV})^2 \tag{A.7}$$

and

$$\phi_1^i(t_e) = \delta_1^i, c_1(t_e) = -10^3\ \mathrm{GeV}, \tag{A.8}$$

taken from Eq. (A.3), we obtain the mapped condition functions as the solutions of Eq. (A.6).

Notice that a mapped condition function that is equal to a dimensionful parameter at t_e, as

$$\phi(t_e) = m_i^2 \text{ or } \phi(t_e) = M_i, \tag{A.9}$$

is a solution of the RG equation with an explicit form in terms of the dimensionful parameters at t. These solutions can actually be obtained by solving Eq. (A.6) with the proper initial conditions imposed where $c_1(t) = c_2(t) = 0$. Finally, substituting all the solutions corresponding to the parameters at t_e, we can map any condition functions to the parameter space at an arbitrary scale t.

References

[1] G. Aad et al. [ATLAS Collaboration], Phys. Lett. B **716**, 1 (2012) [arXiv:1207.7214 [hep-ex]] [Search INSPIRE].
[2] S. Chatrchyan et al. [CMS Collaboration], Phys. Lett. B **716**, 30 (2012) [arXiv:1207.7235 [hep-ex]] [Search INSPIRE].
[3] CMS collaboration, CMS supersymmetry physics results (available at: https://twiki.cern.ch/twiki/bin/view/CMSPublic/PhysicsResultsSUS, date last accessed August 4, 2017).
[4] ATLAS collaboration, supersymmetry searches webpage (available at: https://twiki.cern.ch/twiki/bin/view/AtlasPublic/SupersymmetryPublicResults, date last accessed August 4, 2017).
[5] Y. Okada, M. Yamaguchi, and T. Yanagida, Prog. Theor. Phys. **85**, 1 (1991).
[6] J. Ellis, G. Ridolfi, and F. Zwirner, Phys. Lett. B **257**, 83 (1991).
[7] H. E. Haber and R. Hempfling, Phys. Rev. Lett. **66**, 1815 (1991).
[8] T. Hahn, S. Heinemeyer, W. Hollik, H. Rzehak, and G. Weiglein, Phys. Rev. Lett. **112**, 141801 (2014) [arXiv:1312.4937 [hep-ph]] [Search INSPIRE].
[9] M. Frank, T. Hahn, S. Heinemeyer, W. Hollik, H. Rzehak, and G. Weiglein, J. High Energy Phys. **02**, 047 (2007) [arXiv:hep-ph/0611326] [Search INSPIRE].
[10] G. Degrassi, S. Heinemeyer, W. Hollik, P. Slavich, and G. Weiglein, Eur. Phys. J. C **28**, 133 (2003) [arXiv:hep-ph/0212020] [Search INSPIRE].
[11] S. Heinemeyer, W. Hollik, and G. Weiglein, Eur. Phys. J. C **9**, 343 (1999) [arXiv:hep-ph/9812472] [Search INSPIRE].
[12] S. Heinemeyer, W. Hollik, and G. Weiglein, Comput. Phys. Commun. **124**, 76 (2000) [arXiv:hep-ph/9812320] [Search INSPIRE].
[13] H. Baer and C. Balázs, J. Cosmol. Astropart. Phys. **05**, 006 (2003) [arXiv:hep-ph/0303114] [Search INSPIRE].
[14] J. Ellis, K. A. Olive, Y. Santoso, and V. C. Spanos, Phys. Rev. D **69**, 095004 (2004) [arXiv:hep-ph/0310356] [Search INSPIRE].
[15] P. Bechtle, K. Desch, and P. Wienemann, Comput. Phys. Commun. **174**, 47 (2006) [arXiv:hep-ph/0412012] [Search INSPIRE].
[16] E. A. Baltz and P. Gondolo, J. High Energy Phys. **10**, 052 (2004) [arXiv:hep-ph/0407039] [Search INSPIRE].
[17] Y. Akrami, P. Scott, J. Edsjö, J. Conrad, and L. Bergström, J. High Energy Phys. **04**, 057 (2010) [arXiv:0910.3950 [hep-ph]] [Search INSPIRE].
[18] B. C. Allanach, Phys. Lett. B **635**, 123 (2006) [arXiv:hep-ph/0601089] [Search INSPIRE].
[19] R. Ruiz de Austri, R. Trotta, and L. Roszkowski, J. High Energy Phys. **05**, 002 (2006) [arXiv:hep-ph/0602028]] [Search INSPIRE].
[20] R. Trotta, F. Feroz, M. Hobson, L. Roszkowski, and R. Ruiz de Austri, J. High Energy Phys. **12**, 024 (2008) [arXiv:0809.3792 [hep-ph]] [Search INSPIRE].
[21] V. Berezinsky, A. Bottino, J. Ellis, N. Fornengo, G. Mignola, and S. Scopel, Astropart. Phys. **5**, 1 (1996) [arXiv:hep-ph/9508249] [Search INSPIRE].
[22] M. Drees, M. M. Nojiri, D. P. Roy, and Y. Yamada, Phys. Rev. D **56**, 276 (1997); **64**, 039901(E) (2001) [erratum] [arXiv:hep-ph/9701219] [Search INSPIRE].
[23] P. Nath and R. Arnowitt, Phys. Rev. D **56**, 2820 (1997) [arXiv:hep-ph/9701301] [Search INSPIRE].
[24] G. W. Bennett et al. [Muon g-2 Collaboration], Phys. Rev. D **73**, 072003 (2006) [arXiv:hep-ex/0602035] [Search INSPIRE].
[25] K. Hagiwara, R. Liao, A. D. Martin, D. Nomura, and T. Teubner, J. Phys. G **38**, 085003 (2011) [arXiv:1105.3149 [hep-ph]] [Search INSPIRE].
[26] M. Davier, A. Hoecker, B. Malaescu, and Z. Zhang, Eur. Phys. J. C **71**, 1515 (2011); **72**, 1874 (2012) [erratum] [arXiv:1010.4180 [hep-ph]] [Search INSPIRE].
[27] S. P. Martin and M. T. Vaughn, Phys. Rev. D **50**, 2282 (1994); **78**, 039903(E) (2008) [erratum] [arXiv:hep-ph/9311340] [Search INSPIRE].
[28] I. Jack and D. R. T. Jones, Phys. Lett. B **333**, 372 (1994).
[29] Y. Yamada, Phys. Rev. D **50**, 3537 (1994) [arXiv:hep-ph/9401241] [Search INSPIRE].
[30] M. Drees and M. M. Nojiri, Nucl. Phys. B **369**, 54 (1992).
[31] B. C. Allanach, D. P. George, and B. Gripaios, J. High Energy Phys. **07**, 098 (2013) [arXiv:1304.5462 [hep-ph]] [Search INSPIRE].

[32] B. C. Allanach, D. P. George, and B. Nachman, J. High Energy Phys. **02**, 031 (2014) [arXiv:1311.3960 [hep-ph]] [Search INSPIRE].
[33] T. Moroi, Phys. Rev. D **53**, 6565 (1996) [arXiv:hep-ph/9512396] [Search INSPIRE].
[34] J. L. Lopez, D. V. Nanopoulos, and X. Wang, Phys. Rev. D **49**, 366 (1994) [arXiv:hep-ph/9308336] [Search INSPIRE].
[35] M. Carena, G. F. Giudice, and C. E. M. Wagner, Phys. Lett. B **390**, 234 (1997) [arXiv:hep-ph/9610233] [Search INSPIRE].
[36] H. Baer, V. Barger, and A. Mustafayev, Phys. Rev. D **85**, 075010 (2012) [arXiv:1112.3017 [hep-ph]] [Search INSPIRE].
[37] D. M. Ghilencea, H. M. Lee, and M. Park, J. High Energy Phys. **07**, 046 (2012) [arXiv:1203.0569 [hep-ph]] [Search INSPIRE].
[38] C. Strege, G. Bertone, F. Feroz, M. Fornasa, R. Ruiz de Austri, and R. Trotta, J. Cosmol. Astropart. Phys. **04**, 013 (2013) [arXiv:1212.2636 [hep-ph]] [Search INSPIRE].
[39] O. Buchmueller et al., Eur. Phys. J. C **74**, 3212 (2014) [arXiv:1408.4060 [hep-ph]] [Search INSPIRE].
[40] Y. Shimizu and W. Yin, Phys. Lett. B **754**, 118 (2016) [arXiv:1509.04933 [hep-ph]] [Search INSPIRE].